Ab initio structural and electronic investigation of magnetic *R*NiSn (*R*=La,Ce,Pr,Nd) intermetallics and their hydrides

Andrea Aburto
Departamento de Física, Facultad de Ciencias, Universidad Nacional Autónoma de México, Código Postal 04510, Distrito Federal México, Mexico

Emilio Orgaz
Departamento de Física y Química Teórica, Facultad de Química, Universidad Nacional Autónoma de México, Código Postal 04510, Distrito Federal México, Mexico

(Received 12 October 2006; revised manuscript received 28 November 2006; published 29 January 2007)

We investigated the electronic structure of the *R*NiSn (*R*=La,Ce,Pr,Nd) intermetallic compounds as well as their corresponding mono- and dihydrides. We computed the energy bands and the total and partial densities of states using a mixed approach; a pseudopotential scheme and *ab initio* full potential–all electron band-structure techniques. The crystal structure was investigated for each of the 12 compounds by performing full geometry optimization. We determine the magnetic properties of these compounds. We also analyze the details of the bonding in these systems, in particular, the effect of the hydrogen insertion in the parent intermetallic compounds. We found that, besides the nonmagnetic reference systems $LaNiSnH_x$, the Pr- and Nd-derived systems are consistent with f^{+2} and f^{+3} electronic configurations. The case of the Ce compounds, as expected, showed a more complicated situation; the computed magnetic moment suggests an intermediate valence state for CeNiSnH. The decomposition enthalpies for the mono- and dihydrides have been estimated and compared with experimental values for similar compounds.

DOI: 10.1103/PhysRevB.75.045130 PACS number(s): 71.20.Eh, 71.20.Lp, 71.20.Ps

I. INTRODUCTION

Rare-earth-element-based intermetallics are of particular fundamental interest. The interplay between the chemical composition, crystal structure, and the consequent complex magnetic and electronic behaviors yields a rich field of investigation. This is the case of *R*NiSn (*R*=La,Ce,Pr,Nd) (Refs. 1 and 2) intermetallic compounds and their corresponding hydrides. Intermetallic compounds and their hydrides have attracted enormous research effort during the past decades owing to their interesting physical and chemical properties and their potential use in several applications.[3] In particular, CeNiSn is a special case of 4*f*-heavy fermion system.[4] Although this intermetallic has been characterized to have a valence fluctuating system,[4–6] recent x-rays absorption spectroscopy (XAS) investigations[1] indicates that the main valence state of cerium in this compound is Ce^{III}. Two hydrides derived from CeNiSn have been discovered;[7,8] $CeNiSnH_{\approx 1}$ and $CeNiSnH_{\approx 2}$. While CeNiSnH is an antiferromagnetically ordered phase below around 5 K, $CeNiSnH_2$ is a ferromagnet below 7 K.[7,8] It is worth noting that CeNiSn does not show a magnetic order. The magnetic behavior of CeNiSnH is due to the Ce localized moments. The experimentally determined magnetic moment is 1.37 μ_B by neutron powder diffraction[8] and 0.95 μ_B by magnetic susceptibility measurements,[2] while the contribution of Ni atoms is negligible. In $CeNiSnH_2$, the magnetic moment of Ce has been estimated to be 0.38 μ_B.[7] In both hydrides, the charge state of Ce seems to be Ce^{III} after XAS.[1] Also, the magnetic properties of the La, Pr, and Nd intermetallics have been investigated. LaNiSn is a nonmagnetic intermetallic compound; NdNiSn orders antiferromagnetically below 2.8 K,[9,10] while PrNiSn does not show magnetic order.[9] Some of the corresponding hydrides have been successfully synthesized. The monhydrides of PrNiSn and NdNiSn are known[11,12] as well as the dihydride of LaNiSn.[13] In recent years, we have applied band-structure methods to investigate the magnetic properties of rare-earth-based Laves phases containing a second nonmagnetic element: RM_2 (*R*=rare earth, *M*=Mg,Al).[14] These closely related materials have been fully studied with a methodology similar to that employed in the present investigation and we have found an excellent correlation between the theoretically computed magnetic properties and the reported experimental values. We also employed these methods to the investigation of more complex magnetic hydrides, as in the case of alkali metal–manganese[15] or Mg_3MnH_7.[16]

In this work, we report our results of the systematic investigation of the electronic structure of these series of compounds. We obtained *ab initio* band structure, density of states, and bonding characteristics of these compounds. We include in this investigation the hypothetical hydrides LaNiSnH, $PrNiSnH_2$, and $NdNiSnH_2$.

II. METHODOLOGY

Solid-state electronic structure calculations were carried out using a density-functional theory approach to band theory, employing the generalized gradient approximation[17] (GGA) to the local spin density. To improve the description of the strongly correlated *R*-*f* electrons, we introduce the DFT+$U(J)$ (Ref. 18) correction for the Ce, Pr, and Nd

TABLE I. Lattice parameters (in Å) obtained after full geometry optimization. Data for the *R*NiSn, *R*niSnH, and *R*NiSnH_2 compounds are given in the orthorhombic *Pnma*, *Pna*2_1, and *Pnma* settings, respectively. Index (a) indicates that only the experimental lattice parameters are available, (b) the full crystallographic data are available, and (c) no experimental data are available. The percent shifts relative to the known experimental information are shown.

	a	*b*	*c*	Δ*a*%	Δ*b*%	Δ*c*%
LaNiSn[(a)a]	7.7672	4.7409	7.3215	1.1	1.7	−3.8
CeNiSn[(a)b,c]	7.3742	4.5867	7.5763	−2.2	−0.3	−0.8
PrNiSn[(a)d]	7.6000	4.6838	7.4395	1.7	2.4	−3.1
NdNiSn[(b)d,e]	7.5051	4.6557	7.4835	1.3	2.4	−2.7
LaNiSnH[(c)]	7.2601	8.6465	4.4878			
CeNiSnH[(b)b,f]	7.2271	8.3367	4.3596	−0.6	−1.9	−1.0
PrNiSnH[(a)d]	7.2755	8.5095	4.4373	0.5	0.9	1.4
NdNiSnH[(b)d,e]	7.1986	8.4372	4.4301	−0.3	0.5	1.7
LaNiSnH_2[(b)a]	8.6371	4.4767	7.6389	−0.4	1.2	−0.3
CeNiSnH_2[(a)g]	8.3364	4.3823	7.5483	−2.5	−2.6	−1.5
PrNiSnH_2[(c)]	8.4811	4.4637	7.5900			
NdNiSnH_2[(c)]	8.4120	4.4478	7.5332			

[a]Reference 13.
[b]Reference 1.
[c]Reference 8.
[d]Reference 12.
[e]Reference 11.
[f]Reference 2.
[g]Reference 7.

compounds. We selected fixed reasonable values for *U* and *J* parameters;[19,20] $U=5$ eV and $J=1$ eV. In order to obtain fast and accurate geometry optimization of the crystal structures, we employed a pseudopotential scheme. The projected-augmented plane-wave (PAW) method was used[21,22] (VASP code). We have carried out full geometry optimizations of the 12 intermetallic compounds and hydrides. We relaxed the spatial group constraints to a low symmetry group in order to increase the degrees of freedom during the optimizations. In this research, we did not take into account the observed, in some cases significant, mutual substitution between Ni and Sn atoms in the structure.[1] Geometry equilibria were obtained when a minimum is reached in the total energy and local forces are 10^{-3} eV/Å. This accuracy for local forces introduces an uncertainty of 10^{-3} in the relative coordinates for each nonequivalent atom in the structure. The energy cutoff for plane-wave expansion was set to around 400 eV in order to guarantee the best accuracy in the total energy. All the compounds were investigated in the spin-polarized approximation.

This set of computations was completed by the calculation of the electronic structure of the previously optimized structures by means of the full potential–linear-augmented plane-waves (LAPW) method[23] (WIEN code). The muffin-tin radii were set to 2.30, 1.80, 2.30, and 1.0 a.u. for the rare earth, nickel, tin, and hydrogen atoms, respectively. The RK_{max} parameter, which controls the plane-wave expansion, was selected in order to obtain converged eigenvalues up to 10^{-4} eV. We used RK_{max} of 7.0 and 4.0 for the intermetallics and hydrides, respectively. The sampling of the irreducible wedges of the corresponding Brillouin zones was done by choosing up to 150 **k** points for which we computed the energy eigenvalues. The total density of states (DOS) as well as the angular momentum resolved density of states (PDOS) at each atomic site were computed by the standard tetrahedron integration scheme. The reported magnetic moments were computed by the integration of the density charge at each atomic site. Owing to the accuracy of the employed methods, the integration of the DOS yield similar values.

III. RESULTS AND DISCUSSION

In Table I, we summarize the results of the geometry optimizations of the 12 intermetallic compounds and hydrides. We show the final lattice parameters, indicating the shift from the experimental values. In Table II, the nonequivalent atomic coordinates relative to the lattice parameters are reported. The optimized geometries of the intermetallic compounds and their known hydrides are generally in good agreement with the experimental data. This give us enough confidence in order to investigate the magnetic phases as well as to propose a crystal structure and parameters for the not yet reported hydrides: LaNiSnH, PrNiSnH_2, and

TABLE II. Relative coordinates for the geometry optimized intermetallic compounds and their hydrides. *R*NiSn, *R*NiSnH, and *R*NiSnH_2 data are referred to the *Pnma*, *Pna*2_1, and *Pnma* space group settings, respectively.

	*R*NiSn			*R*NiSnH			*R*NiSnH_2		
	x	*y*	*z*	*x*	*y*	*z*	*x*	*y*	*z*
La	0.9694	0.2500	0.6839	0.0094	0.3099	0.2428	0.0005(0.001)	0.2500(0)	0.7503(0.003)
Ni	0.1760	0.2500	0.0743	0.7820	0.9066	0.2427	0.2498(−0.005)	0.2500(0)	0.4194(0.002)
Sn	0.3232	0.2500	0.3993	0.6564	0.5675	0.2428	0.2501(0.008)	0.2500(0)	0.0844(0.006)
H_1				0.4385	0.0824	0.7428	0.9361(0.003)	0.2500(0)	0.0870(−0.010)
H_2							0.5636(0.004)	0.2500(0)	0.0850(−0.002)
Ce	0.9799	0.2500	0.6975	0.0098(0.000)	0.3092(0.003)	0.2428(0.032)	0.0000	0.2500	0.7500
Ni	0.2007	0.2500	0.0780	0.7854(−0.001)	0.8963(−0.004)	0.2427(0.010)	0.2500	0.2500	0.4183
Sn	0.3161	0.2500	0.4077	0.6678(−0.005)	0.5726(−0.003)	0.2428(−0.016)	0.2500	0.2500	0.0840
H_1				0.4413(0.009)	0.0809(0.005)	0.2426(−0.025)	0.9451	0.2500	0.0832
H_2							0.5549	0.2500	0.0831
Pr	0.9737	0.2500	0.6901	0.0160	0.3091	0.2427	0.0003	0.2500	0.7503
Ni	0.1794	0.2500	0.0760	0.7821	0.9019	0.2431	0.2500	0.2500	0.4208
Sn	0.3181	0.2500	0.4028	0.6589	0.5693	0.2430	0.2501	0.2500	0.0845
H_1				0.4384	0.0811	0.7422	0.9304	0.2500	0.0870
H_2							0.5605	0.2500	0.0852
Nd	0.9757(−0.013)	0.2500(0)	0.6934(−0.007)	0.0130(0.002)	0.3096(0.001)	0.2427(−0.001)	0.0004	0.2500	0.7501
Ni	0.1840(−0.016)	0.2500(0)	0.0763(−0.007)	0.7798(0.000)	0.9024(0.002)	0.2429(0.000)	0.2500	0.2500	0.4208
Sn	0.3162(0.002)	0.2500(0)	0.4043(−0.008)	0.6589(0.000)	0.5699(0.000)	0.2428(0.000)	0.2499	0.2500	0.0843
H_1				0.4420(0.000)	0.0811(0.000)	0.7427(0.000)	0.9413	0.2500	0.0871
H_2							0.5586	0.2500	0.0848

$NdNiSnH_2$. We start the description of the electronic structure of these compound series with the $LaNiSnH_x$ systems. In Fig. 1, we plotted the total and partial DOSs obtained for LaNiSn. This intermetallic compound is found to be nonmagnetic. The characteristic total DOS of this compound reflects the different orbital interactions in the solid.

The first structure, in increasing order of energy, is constituted by states concerning essentially the Sn-*s* orbitals, which interact with La-*s*,*p* and Ni-*s* orbitals. This can be appreciated in the same energy range in the PDOS plots at the La, Ni, and Sn sites [Figs. 1(b)–1(d)]. The inspection of the wave-function coefficients (not shown) at the center of the Brillouin zone (Γ $\vec{k}$ point) supports this interpretation. This first structure in the DOS is well separated (≈2 eV) from a strong manifold, which is constituted by the Sn-*p*/La-*d* and marginally Ni-*s* in the range of −4.5–−3 eV below the Fermi energy. This is continuously followed by the strong Ni-*d* states with contributions from the La-*p* and Sn-*p* orbitals. This description stays for the entire intermetallic series. The states at the Fermi energy arise from the Ni-*d*/La-*d*/Sn-*p* orbital interactions. This compound exhibits a DOS/f.u. at Fermi energy (E_F) of 3.34 states/f.u. eV and a small specific heat coefficient γ =3.94 mJ/(mol f.u. K^2). In Table III, we summarize the density of states at the Fermi energy along with the computed γ values and magnetic moments for all the compounds under investigation.

In Fig. 2, we plot the total DOS and the atomic site contributions to the DOS for CeNiSn. The main differences in the electronic structure arise from the 4*f* states in the Ce-based compound. This observation is common to all the intermetallics for which the most relevant differences arise from the position of the 4*f* energy bands. The DOS at Fermi energy for CeNiSn changes slightly with respect to the La-based intermetallic. We found that the DOS at E_F are 1.23(1.31) states/(f.u. eV spin) for spin up (down) and γ takes the values 2.90(3.10) mJ/(mol f.u. K^2) spin. The main orbital contributions at this energy remain Ni-*d*/Ce-*d*/Sn-*p* with a nonhybridized small contribution from Ce-*f* spin up, which appears at 1.5 eV below the Fermi level.

In Fig. 3, we compare the total DOS along with the PDOS at the H atomic site for both La-derived hydrides. The general features of the electronic structure are maintained with respect to the La-based intermetallic. However, the insertion of H in the intermetallic modifies the local symmetry and introduces new states at around 6 eV below the Fermi energy. In Figs. 3(a) and 3(b), the total DOS shows the Ni-*d*/H-*s* states (labeled in the plots), which are 1.2 eV wide in the monohydride and ≈3 eV in the dihydride. The local environment of Ni in LaNiSnH consists of one H atom at 1.61 Å and four Sn atoms at distances ranging from

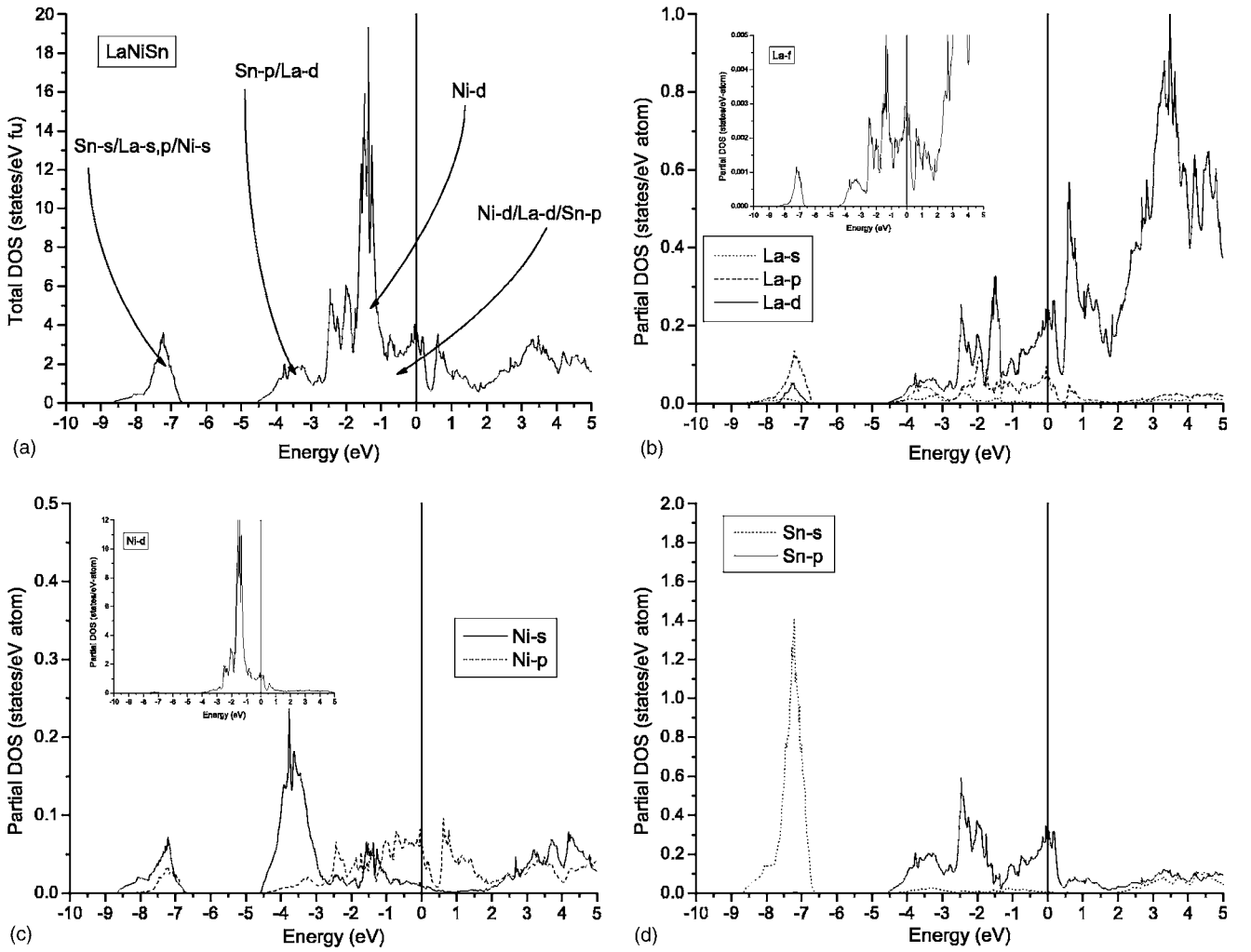

FIG. 1. (a) Total density of states (in states/eV f.u.) of LaNiSn intermetallic compound, and atomic site-projected density of states (in states/eV at.) for (b) lanthanum, (c) nickel, and (d) tin. The origin of the energy scale corresponds to the Fermi energy.

2.57 to 2.86 Å. In the dihydride, this local environment contains the same number of neighbors but now two H atoms at essentially the same distance and three Sn atoms at 2.6 Å. The increase in the number of H neighbors around the nickel atom at short distances increases the band dispersion, increasing the computed bandwidth. The DOS at E_F decreases on hydrogenation being 2.52 and 1.84 states/f.u. eV for LaNiSnH and $LaNiSnH_2$, respectively. The small γ values follow the same trend (see Table III).

Ce-based compounds are known to challenge the electronic structure methods,[24–26] owing to the particular behavior of the high electron correlation of the 4*f* states. Ce shows frequently a +3 state; however, it is not rare to find oxidized Ce^{+4} in a large number of compounds. With the same GGA+$U(J)$ approach and parametrization for the three Ce compounds, the position of Ce-4*f* states with respect to the Fermi energy changes from −1.5 eV for the intermetallic to values close to the E_F for the hydrides. As a consequence, the DOSs at E_F are very different for the hydrogenated Ce compounds (Figs. 4 and 5). We found that the contribution at E_F from Ce-*f* states rises from 0.03(0.00) states/eV at. for CeNiSn to 0.31(0.03) and 1.33(0.00) for CeNiSnH and

TABLE III. Density of states at the Fermi energy (states/eV f.u.), electronic specific heat coefficient [mJ/(mol f.u. K^2)], magnetic moment μ per formula, and magnetic moment contribution of the rare earth μ_R (in μ_B) for the intermetallic compounds and corresponding hydrides. For the La compounds, the density of states and specific heat coefficients are reported for both spins. For the Ce, Pr, and Nd compounds, these figures are reported for each spin direction; spin up and spin down in parentheses.

	$n(E_F)$	γ	μ	μ_R
LaNiSn	3.34	3.94	0.0	0.0
LaNiSnH	2.52	2.98	0.0	0.0
$LaNiSnH_2$	1.84	2.17	0.0	0.0
CeNiSn	1.23(1.31)	2.90(3.10)	1.068	0.964
CeNiSnH	2.38(1.65)	5.60(3.89)	0.573	0.283
$CeNiSnH_2$	9.30(0.78)	21.91(1.85)	0.975	0.851
PrNiSn	1.29(1.27)	3.04(2.99)	2.138	1.999
PrNiSnH	1.64(0.31)	3.86(0.74)	2.146	2.016
$PrNiSnH_2$	0.99(1.13)	2.33(2.66)	2.145	2.016
NdNiSn	2.50(1.63)	5.90(3.85)	3.409	3.160
NdNiSnH	1.82(0.49)	4.29(1.15)	3.270	3.140
$NdNiSnH_2$	7.67(0.99)	18.07(2.35)	3.447	3.235

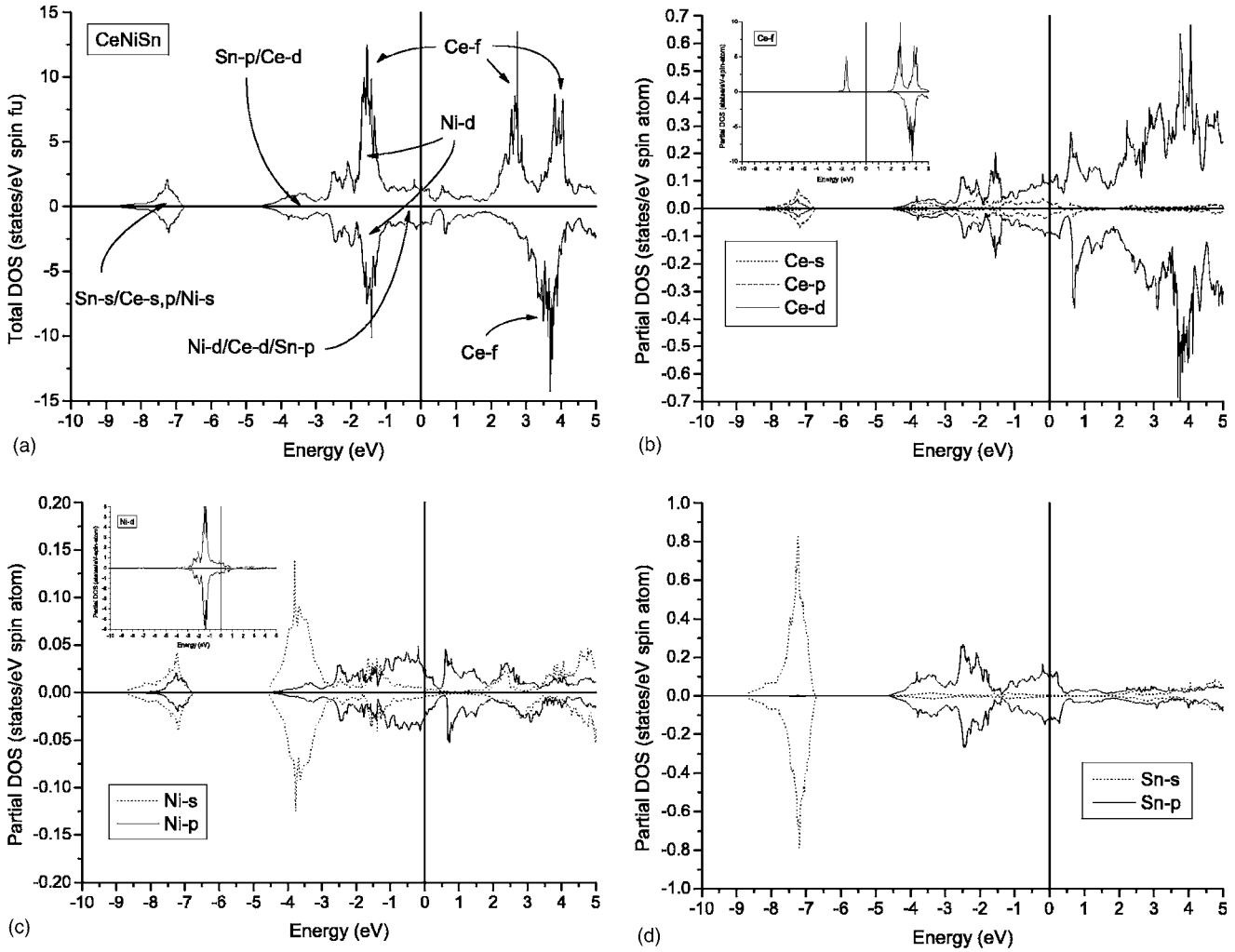

FIG. 2. (a) Total density of states [in states/(spin eV f.u.)] of CeNiSn intermetallic compound, and atomic site-projected density of states [in states/(spin eV at.)] for (b) cerium, (c) nickel, and (d) tin. The origin of the energy scale corresponds to the Fermi energy.

$CeNiSnH_2$, respectively, for each spin state. These contributions increase the total DOS at E_F, while the Ni-d/Ce-d/Sn-p interaction remains essentially constant. This is a consequence of the valence H states, which shift the Fermi level. The calculated magnetic moments of the compounds are summarized in Table III. It is interesting to note that, under the same approximations, CeNiSnH shows a smaller magnetic moment. We obtain for the Ce compounds magnetic moments of 0.96, 0.28, and 0.85 μ_B for CeNiSn, CeNiSnH, and $CeNiSnH_2$, respectively. In these compounds, the Ni atomic contribution to magnetism is negligible except in the case of CeNiSnH, where Ni exhibits a magnetic moment of 0.27 μ_B. Our estimates of the magnetic moment for CeNiSnH are surprising, owing to the observed consistency of the electronic results for the full $RNiSnH_x$ ($x=0,1,2$) series. CeNiSn and $CeNiSnH_2$ show localized Ce-f states occupied by one electron indicating a Ce^3 state. This consistency (see below) is maintained for the Pr and Nd compounds, indicating f^{+2} and f^{+3} states, respectively. The special case of CeNiSnH involves a significant contribution of the Ni-3d states to magnetism. Looking to the structural properties, we find that the Ce compounds show similarities that do not permit, in the first instance, explaination of this particular behavior. The Ce-Ce distances in these compounds are 3.77, 3.74, and 4.27 Å for CeNiSn, CeNiSnH, and $CeNiSnH_2$, respectively. The Hill criteria[27] for magnetic order ($d_{\text{Ce-Ce}}=3.4$ Å) do not apply in this series of compounds; the Ce-Ce distances in the intermetallic and monohydride are relatively close to this critical distance. However, CeNiSn does not show magnetic order and CeNiSnH is a weak antiferromagnet. The suppression of the Ce magnetic moment and the concurrent enhancement of that from Ni atoms in CeNiSnH could suggest an intermediate charge state for Ce between Ce^{+3} and Ce^{+4}.

For NdNiSn, we found that the Nd-f PDOS splits for the spin up (down) roughly 1.0 eV (0.6 eV) between the occupied and unoccupied peaks. The occupied peak $\left(j=\frac{5}{2}\right)$ of the Nd-f (spin up) is located at 0.6 eV below the Fermi energy, while the first unoccupied peak of the Nd-f PDOS for the spin down appears at 1.6 eV above the Fermi level. These states are relatively close to the Fermi energy and are con-

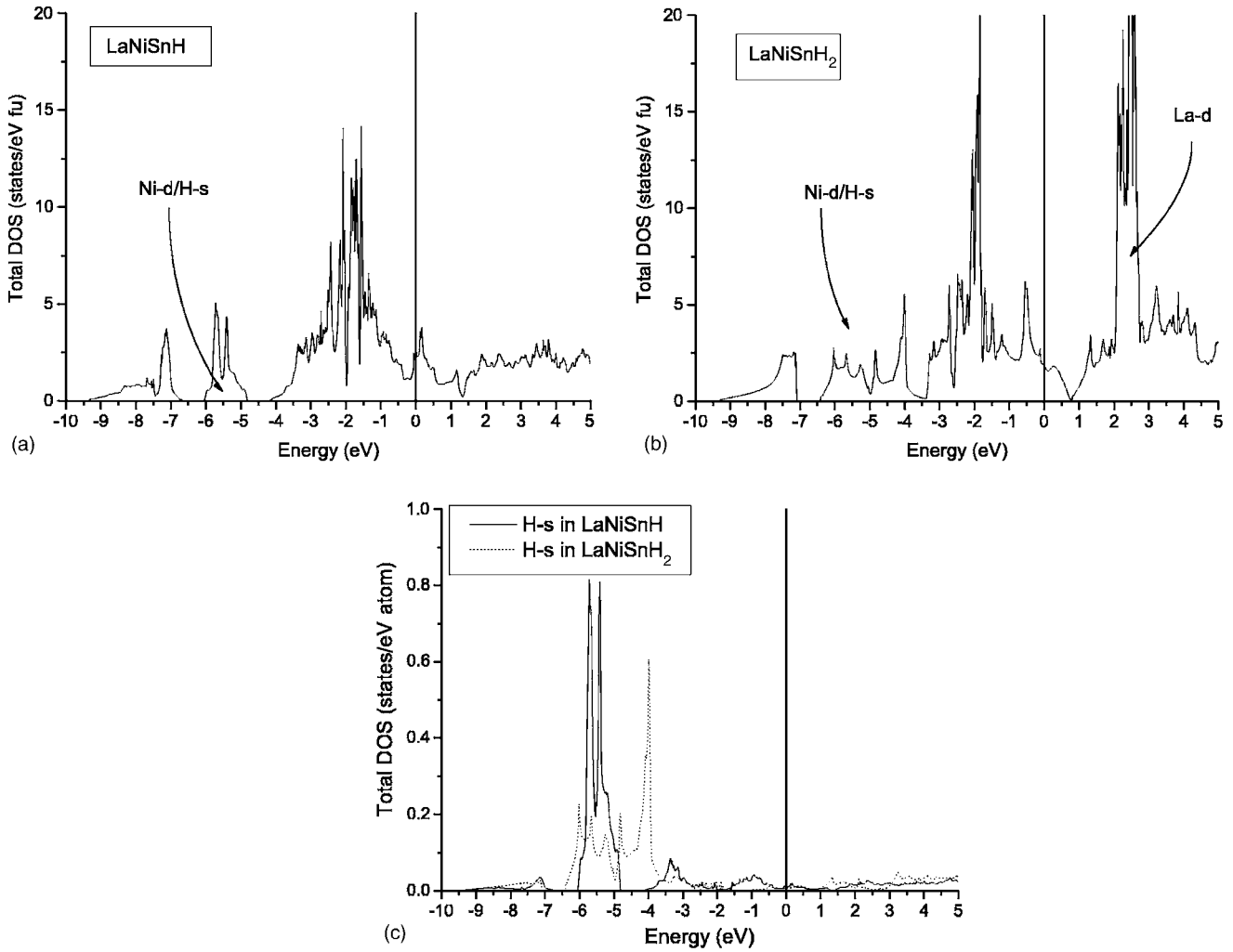

FIG. 3. Total density of states (in states/eV cell) of (a) LaNiSnH, (b) $LaNiSnH_2$, and (c) atomic site-projected density of states (in states/eV at.) for H-*s* in LaNiSnH and $LaNiSnH_2$. The origin of the energy scale corresponds to the Fermi energy.

sistent with our results on $NdAl_2$,[14] but they are different when compared to the results of the band structure reported by Spataru *et al.*[28] By employing the same method and essentially the same parametrization for the U and J parameters, they found that the Nd-*f* occupied states appeared at 4 eV below the Fermi energy. In recent electronic structure investigations on molybdenum-based pyroclore systems ($Nd_2Mo_2O_7$) employing the linear muffin-tin orbital method and essentially the same approach to the LSD+$U(J)$ correction, the authors[20] found that the Nd-*f* localized band appeared at 2 eV below the Fermi energy, a situation similar to the systems investigated in this work. One possible reason for this difference is the employed DFT+U approximation. In our case, we set GGA+$U(J)$ corrections while in the work of Spataru *et al.*, the LDA+$U(J)$ technique was performed. As it has been recently pointed out,[24–26] these different approaches yield different results for the R-4*f* band position. Moreover, it seems that the effective Hubbard parameters (defined by Hubbard as U and J) are not so easily transferable from one compound to other.

For the derived hydrides, the Nd-*f* structure preserves the *valence-conduction-band* splittings but shifted towards higher energies by ≈0.2 and ≈0.4 eV for NdNiSnH and $NdNiSnH_2$, respectively. We obtained a strong magnetic moment for the Nd compounds, attaining essentially 3.1 μ_B for the three compounds. This result is clearly consistent with the ideal magnetic moment for Nd^{+3} observed, for example, in $NdAl_2$.[14] The electronic structure of the Pr-based compounds follows the same trends. The overall contributions match those observed for La compounds. The results for the Pr-based compounds show a localized Pr-*f* band at around 2.5 eV below the Fermi energy and a magnetic moment indicating Pr^{+3}. This result is similar to those obtained in several compounds.[14,29]

We computed the decomposition energies (enthalpies) for the mono- and dihydrides (Fig. 6). We considered three decomposition reactions (a) from the dihydride, $RNiSnH_2 \rightarrow RNiSn+H_2$, (b) from the monohydride, $RNiSnH \rightarrow RNiSn+\frac{1}{2}H_2$, and (c) the partial decomposition, $RNiSnH_2 \rightarrow RNiSnH+\frac{1}{2}H_2$. The decomposition enthalpies were computed as a difference of the total electronic ener-

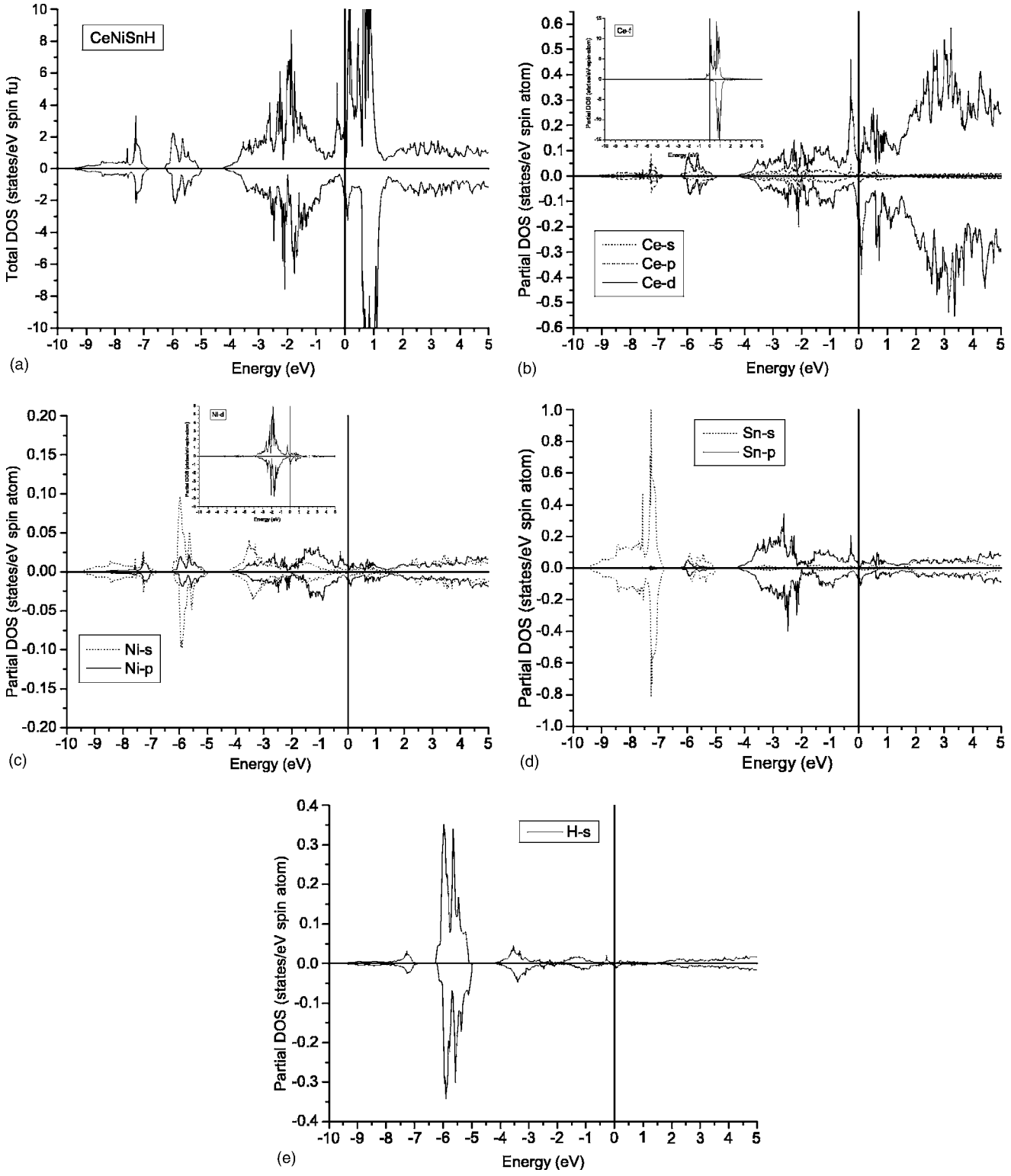

FIG. 4. (a) Total density of states [in states/(spin eV f.u.)] of CeNiSnH intermetallic hydride, and atomic site-projected density of states [in states/(spin eV at.)] for (b) cerium, (c) nickel, (d) tin, and (e) hydrogen. The origin of the energy scale corresponds to the Fermi energy.

gies. For consistency, all the total energies (for the solid systems as well as for the H_2 molecule) were calculated within the same approximations (VASP code). These results are summarized in Fig. 4. The calculated enthalpies are consistent with the experimentally observed values[30] for similar compounds. The observed trends along the lanthanide series indicate a small decrease in these figures as the volume cell reduces. This is consistent with the lanthanide contraction,

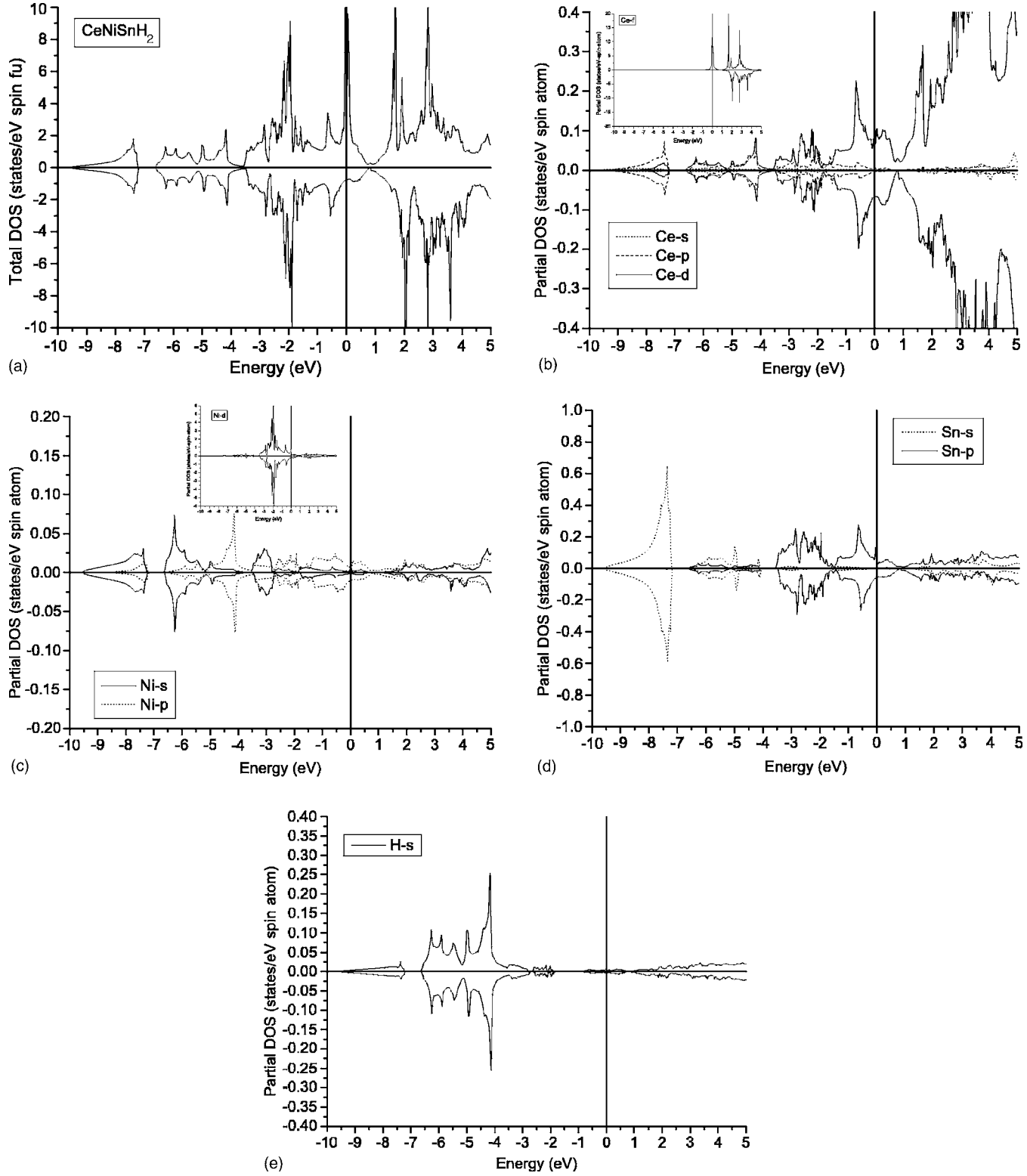

FIG. 5. (a) Total density of states [in states/(spin eV f.u.)] of $CeNiSnH_2$ intermetallic hydride, and atomic site-projected density of states [in states/spin eV at.] for (b) cerium, (c) nickel, (d) tin, and (e) hydrogen. The origin of the energy scale corresponds to the Fermi energy.

making it more difficult to insert interstitial H atoms in the structure. However, as pointed out by Griessen and Riesterer,[30] it is not always possible to establish a clear correlation between the hydride formation energy and structural parameters. For the hydrides under investigation, the experimental formation enthalpies are unknown. Experimental values are known for similar systems as $LaNi_5H_6$, $LaNi_2H_2$, $LaNiH_4$, and La_3NiH_2, having formation enthalpies of −32,

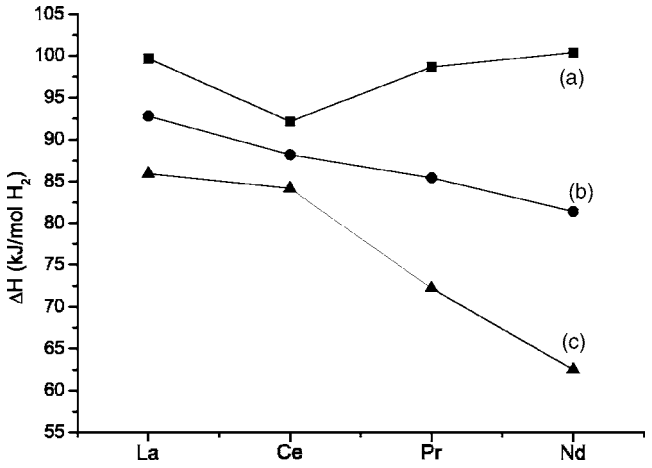

FIG. 6. Enthalpy of hydride decomposition (in kJ/mol H_2) computed ab initio from the PAW method results. Three reactions are considered (a) filled squares, $R\mathrm{NiSnH} \rightarrow R\mathrm{NiSn} + \frac{1}{2}\mathrm{H}_2$, (b) filled circles, $R\mathrm{NiSnH}_2 \rightarrow R\mathrm{NiSn} + \mathrm{H}_2$, and (c) filled triangles, $R\mathrm{NiSnH}_2 \rightarrow R\mathrm{NiSnH} + \frac{1}{2}\mathrm{H}_2$.

−54, −126, and −222 kJ/mol H_2,[30] respectively. Our results for the formation enthalpies of *R*NiSnH and $R\mathrm{NiSnH}_2$ are consistent with those observed for other hydrides.

IV. CONCLUSIONS

We have investigated the electronic structure of *R*NiSn intermetallics along with the known derived hydrides. After a full geometry optimization of the crystal structure, we computed the total and partial density of states *ab initio*. These properties along with the wave-function coefficient analysis at the center of the respective Brillouin zones permit us to establish the main orbital contributions to the bonding. The computed magnetic properties of these compounds indicate that the Pr- and Nd-derived compounds are consistent with f^{+2} and f^{+3} electronic structures. We are able to reproduce the observed magnetic moments which are similar to the ideal theoretical values for +3 cations. The case of the Ce compounds suggests an intermediate valence situation for CeNiSnH. Finally, we estimate the decomposition energies for the mono- and dihydrides. We found decomposition enthalpies indicative of strong metal-hydrogen interactions.

ACKNOWLEDGMENTS

Financial support was provided by DGAPA-UNAM under Grant No. IN102202. We would like to thank DGSCA-UNAM for providing us the computing facilities.

[1] M. Stange, V. Paul-Boncour, M. Latroche, A. Percheron-Guégan, O. Isnard, and V. A. Yartys, J. Alloys Compd. **404**, 144 (2005).
[2] B. Chevalier, M. Pasturel, J.-L. Bobet, R. Decourt, J. Etourneau, J. Sanchez Marcos, and J. Rodriguez Fernandez, J. Alloys Compd. **383**, 4 (2004).
[3] P. Dantzer, in *Hydrogen in Metals III*, Topics in Applied Physics Vol. 73, edited by H. Wipf (Springer, Berlin, 1997), p. 273.
[4] A. Ślebarski, A. Jezierski, A. Zygmunt, S. Mähl, M. Neumann, and G. Borstel, Phys. Rev. B **54**, 13551 (1996).
[5] A. Ślebarski, M. Orzechowska, A. Wrona, J. Szade, and A. Jezierski, J. Phys.: Condens. Matter **12**, 1269 (2000).
[6] T. Takabatake, F. Teshima, H. Fujii, S. Nishigori, T. Suzuki, T. Fujita, Y. Yamaguchi, and J. Sajurai, Phys. Rev. B **41**, 9607 (1990).
[7] B. Chevalier, J.-L. Bobet, M. Pasturel, E. Bauer, F. Weill, R. Decourt, and J. Etourneau, Chem. Mater. **15**, 2118 (2003).
[8] V. A. Yartys, B. Ouladdiaf, O. Isnard, O. Yu. Khyzhun, and K. H. J. Buschow, J. Alloys Compd. **359**, 62 (2003).
[9] M. Kurisu, R. Hara, G. Nakamoto, Y. Andoh, S. Kawano, and D. Scmitt, Physica B **312**, 861 (2002).
[10] B. Chevalier, F. Fourgeot, L. Fournès, P. Gravereau, G. Le Caër, and J. Etourneau, Physica B **226**, 283 (1999).
[11] V. A. Yartys, T. Olavesen, B. C. Hauback, and H. Fjellvåg, J. Alloys Compd. **336**, 181 (2002).
[12] T. Spataru, G. Principi, V. Kuncser, W. Keune, and V. A. Yartys, J. Alloys Compd. **366**, 81 (2004).
[13] V. A. Yartys, T. Olavesen, B. C. Hauback, H. Fjellvåg, and H. W. Brinks, J. Alloys Compd. **330–332**, 141 (2002).
[14] E. Orgaz, J. Alloys Compd. **322**, 45 (2001).
[15] E. Orgaz, Phys. Rev. B **61**, 7989 (2000).
[16] E. Orgaz and M. Gupta, Int. J. Quantum Chem. **80**, 141 (2000).
[17] J. P. Perdew, K. Burke, and M. Ernzerhof, Phys. Rev. Lett. **77**, 3865 (1996).
[18] V. I. Anisimov, I. V. Solovyev, M. A. Korotin, M. T. Czyzyk, and G. A. Sawatzky, Phys. Rev. B **48**, 16929 (1993).
[19] J. F. Herbst, R. E. Watson, and J. W. Wilkins, Phys. Rev. B **17**, 3089 (1978).
[20] J.-S. Kang, Y. Moritomo, Sh. Xu, C. G. Olson, J. H. Park, S. K. Kwon, and B. I. Min, Phys. Rev. B **65**, 224422 (2002).
[21] G. Kresse and J. Hafner, Phys. Rev. B **47**, 558 (1993); G. Kresse and J. Furthmuller, Comput. Mater. Sci. **6**, 15 (1996).
[22] P. E. Blöchl, Phys. Rev. B **50**, 17953 (1994); G. Kresse and D. Joubert, *ibid.* **59**, 1758 (1999).
[23] P. Blaha, K. Schwarz, G. K. H. Madsen, D. Kvasnicka, and J. Luitz, *WIEN2k: An Augmented Plane Wave + Local Orbitals Program for Calculating Crystal Properties* (Technische Universität Wien, Austria, 2001).
[24] S. Fabris, S. de Gironcoli, S. Baroni, G. Vicario, and G. Balducci, Phys. Rev. B **71**, 041102 (2005).
[25] G. Kresee, P. Blaha, J. L. F. Da Silva, and M. V. Ganduglia-Pirovano, Phys. Rev. B **72**, 237101 (2005).
[26] S. Fabris, S. de Gironcoli, S. Baroni, G. Vicario, and G. Balducci, Phys. Rev. B **72**, 237102 (2005).
[27] H. H. Hill, Nucl. Metall. **12**, 2 (1970).
[28] T. Spataru, P. Palade, G. Principi, V. Kuncser, S. Lo Russo, S. dal Toé, and V. A. Yartys, J. Chem. Phys. **122**, 124703 (2005).
[29] L. Petit, A. Svane, Z. Szotek, and W. M. Temmerman, Phys. Rev. B **72**, 205118 (2005).
[30] R. Griessen and T. Riesterer, in *Hydrogen in Intermetallic Compopunds I*, Topics in Applied Physics Vol. 63, edited by L. Schlapbach (Springer, Berlin, 1988).